

FROM ELASTIC SCATTERING TO CENTRAL EXCLUSIVE PRODUCTION: PHYSICS WITH FORWARD PROTONS AT RHIC* **

WŁODEK GURYN

Brookhaven National Laboratory, Upton, NY 11973-5000, USA

(Received February 24, 2021; accepted March 8, 2021)

We describe a physics program at the Relativistic Heavy Ion Collider (RHIC) with tagged forward protons. The program started with the proton–proton elastic scattering experiment (PP2PP), for which a set of Roman Pot stations was built. The PP2PP experiment took data at RHIC as a dedicated experiment at the beginning of RHIC operations. To expand the physics program to include non-elastic channels with forward protons, such as Central Exclusive Production (CEP), Central Production (CP) and Single Diffraction Dissociation (SD), the experiment with its equipment was merged with the STAR experiment at RHIC. Consequently, the expanded program, which included both elastic and inelastic channels became a part of the physics program and operations of the STAR experiment. In this paper, we shall describe the physics results obtained by the PP2PP and STAR experiments to date.

DOI:10.5506/APhysPolB.52.217

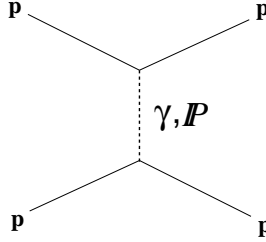
1. Introduction

In the description of the physics program, we shall follow the time-line and evolution of the program from its inception as a PP2PP experiment [1] to the most recent results with the STAR experiment [2]. We start by introducing basic quantities needed to describe elastic scattering.

The proton–proton elastic scattering, Fig. 1, is described by a scattering amplitude which has two components: the electromagnetic part, described by the well-known Coulomb amplitude f_C , and the hadronic part, described

* Prepared for the 60th anniversary of the Cracow School of Theoretical Physics.

** This work was partially supported by the U.S. Department of Energy under contract number de-sc0012704.

Fig. 1. Diagram of pp elastic scattering.

by the hadronic amplitude f_h . The hadronic amplitude is commonly expressed as a function of the center-of-mass energy \sqrt{s} and four-momentum-transfer squared t , which for small scattering angles θ can be expressed as

$$t = (p_{\text{in}} - p_{\text{out}})^2 \approx -p^2\theta^2 = -p^2 (\theta_x^2 + \theta_y^2). \quad (1)$$

The differential elastic pp cross section is expressed as a square of the scattering amplitude

$$\frac{d\sigma_{\text{el}}}{dt} = \pi |f_C + f_h|^2. \quad (2)$$

Thus, the differential cross section $d\sigma_{\text{el}}/dt$ for elastic scattering in the forward angle region is determined by Coulomb and nuclear amplitudes, and the interference term between them. The cross section is given by [3]

$$\begin{aligned} \frac{d\sigma_{\text{el}}}{dt} = & 4\pi (\hbar c)^2 \left(\frac{\alpha G_E^2}{t} \right)^2 + \frac{1 + \rho^2}{16\pi (\hbar c)^2} \sigma_{\text{tot}}^2 e^{-B|t|} \\ & - (\rho + \Delta\Phi) \frac{\alpha G_E^2}{|t|} \sigma_{\text{tot}} e^{-\frac{1}{2}B|t|}, \end{aligned} \quad (3)$$

where α the fine structure constant, G_E the electric form factor of the proton, $\Delta\Phi$ the Coulomb phase [4], ρ the ratio of the real-to-imaginary part of the forward scattering amplitude, σ_{tot} the total cross section, and B the nuclear slope parameter. The first term in Eq. (3) is the Coulomb term, the second is the hadronic term and the third is the so-called Coulomb Nuclear Interference (CNI) term.

At the time of the proposal of the PP2PP experiment, the UA4 experiment [5] published an anomalously large ρ -value. Hence, it was quite natural to propose an experiment at RHIC at $\sqrt{s} = 500$ GeV, which among other things, could measure the ρ -value in proton-proton collisions at a similar to UA4 experiment's $\sqrt{s} = 546$ GeV. Hence, a comprehensive experiment to measure the total and elastic cross sections was proposed for the RHIC physics program.

2. Results from PP2PP experiment

The PP2PP experiment obtained few results on pp elastic scattering at $\sqrt{s} = 200$ GeV. These were the first results from pp elastic scattering above the ISR \sqrt{s} of 63 GeV, the highest \sqrt{s} at the time. The first result was obtained with limited statistics due to the short data-taking time, the B -slope [6] parameter was measured in the small t -range of $0.010 \leq -t \leq 0.019$ GeV² to be $B = 16.3 \pm 1.6$ (stat.) ± 0.9 (syst.) GeV⁻². The error bars were rather large due to the limited statistics of the measurement. Spin dependence in pp elastic scattering was also measured. Both the single-spin asymmetry A_N [7] and double-spin asymmetry A_{NN} [8] were measured in the low- t region, $0.002 < -t < 0.03$ GeV². The A_N in this t -range is sensitive to a possible contribution from the hadronic spin-flip amplitude, which is due to the interference of the Pomeron spin-flip amplitude and electromagnetic non-flip amplitude and would change A_N . The common measure of this effect is the variable r_5 [9, 10], which measures the ratio of hadronic spin-flip to non-flip amplitudes. It was found that the A_N follows the Coulomb Nuclear Interference curve and that the r_5 fitted to the data was compatible with no hadronic spin-flip. The double-spin asymmetry A_{NN} was also found compatible with zero.

3. Results on elastic scattering at STAR

As mentioned earlier, the Roman Pot setup of the PP2PP experiment was subsequently moved to and became part of the STAR to continue pp elastic scattering program and also to expand physics program to include diffractive scattering with tagged forward protons. We start with the results on elastic pp scattering published to date, where two major results were obtained.

The first was an improved result on the A_N , which put a more stringent limit on the hadronic spin-flip amplitude r_5 at $\sqrt{s} = 200$ GeV and was obtained [11] using higher statistics in t -range $0.003 \leq -t \leq 0.035$ GeV², where there is a significant interference between the electromagnetic and hadronic scattering amplitudes. The measured values of A_N and its t dependence are consistent with a vanishing hadronic spin-flip amplitude within 1σ , see Fig. 2, where the real and imaginary parts of r_5 are plotted. The measurement provides a strong constraint on the ratio of the single spin-flip to the non-flip amplitudes. Since the hadronic amplitude is dominated by the Pomeron amplitude at this \sqrt{s} , we conclude that a strong constraint on the presence of a hadronic spin-flip due to the Pomeron exchange in polarized pp elastic scattering was obtained.

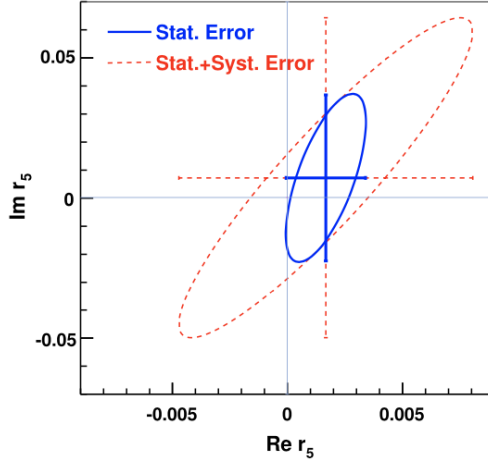


Fig. 2. Fitted value of r_5 , $\text{Im } r_5$ versus $\text{Re } r_5$, with contours corresponding to statistical error (solid ellipse and cross) and statistical + systematic errors added in quadrature (dashed ellipse and cross) of 1σ .

The second was a measurement of the elastic differential cross section measured in the t -range $0.045 \leq -t \leq 0.135 \text{ GeV}^2$ [12]. The results are shown in Fig. 3 and they included the following observables. The value of the exponential slope parameter B of the elastic differential cross section $d\sigma/dt \sim e^{-Bt}$ in the measured t -range was found to be $B = 14.32 \pm 0.09$ (stat.) $_{-0.28}^{+0.13}$ (syst.) GeV^{-2} . The total cross section σ_{tot} , obtained from

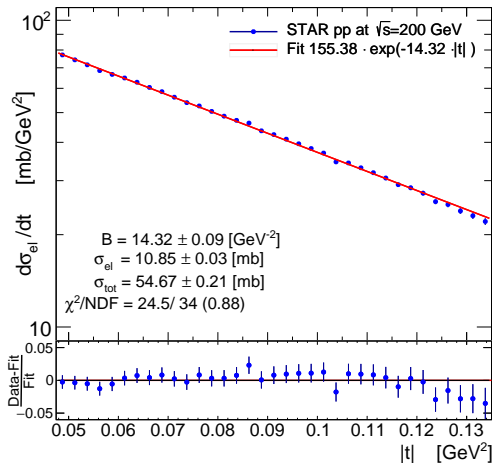


Fig. 3. Top panel: pp elastic differential cross section $d\sigma/dt$ fitted with exponential $A \exp(Bt)$, results are shown; Bottom panel: Residuals (Data-Fit)/Fit. Uncertainties are statistical only.

extrapolation of the $d\sigma/dt$ to the optical point at $t = 0$, is $\sigma_{\text{tot}} = 54.67 \pm 0.21$ (stat.) $_{-1.38}^{+1.28}$ (syst.) mb. Obtained were also the values of the elastic cross section $\sigma_{\text{el}} = 10.85 \pm 0.03$ (stat.) $_{-0.41}^{+0.49}$ (syst.) mb, the elastic cross section integrated within the STAR t -range $\sigma_{\text{el}}^{\text{det}} = 4.05 \pm 0.01$ (stat.) $_{-0.17}^{+0.18}$ (syst.) mb, and the inelastic cross section $\sigma_{\text{inel}} = 43.82 \pm 0.21$ (stat.) $_{-1.44}^{+1.37}$ (syst.) mb. The result on σ_{tot} is the only one on the total cross section at \sqrt{s} between the ISR and the LHC energies. All the results agree well with the world data.

4. Results on central exclusive production at STAR

The major motivation to move the Roman Pot system to STAR was a possibility of combining the measurement of the forward protons with the measurement of the central (recoil) system in the STAR detector, thus allowing the determination of the exclusivity of the final state in $pp \rightarrow pXp$ reaction, where all the particles in the final state are measured. The verification of the exclusivity of that final state is a very unique feature of the results described here, as it is very common to infer exclusivity by requiring rapidity gaps and of a small p_{T} of the final state. The latter is a reasonable approximation of the exclusivity but it is clearly not the same as the measurement of all particles in the final state. In the results described here, the system X consists of hadron pairs of opposite charge $\pi^+\pi^-$, K^+K^- and $p\bar{p}$. We present a brief summary of the results obtained at $\sqrt{s} = 200$ GeV, for a more detailed discussion see [13].

The charged particle pairs' momenta were obtained from the tracks measured in the Time Projection Chamber (TPC) of the central detector. The particle identification (PID) was obtained using the energy loss (dE/dx) measured in the TPC and the time-of-flight measurement in the Time-of-Flight (TOF) system. The forward-scattered protons were reconstructed in the Roman Pot system. Exclusivity of the event was determined by requiring the transverse momentum balance of all four final-state particles to be small $p_{\text{T}}^{\text{miss}} < 75$ MeV/ c . A number of differential cross sections were measured in the fiducial volume of the STAR detector, as a function of various observables of the central hadronic final state and of the forward-scattered protons. This fiducial region roughly corresponds to t -values at the proton vertices (t_1, t_2), in the range of $0.04 < -t_1, -t_2 < 0.2$ GeV 2 , invariant masses M_X of the charged hadron pairs up to a few GeV, and pseudorapidities (η) of the centrally-produced hadrons to be in the acceptance of the TOF system's acceptance $|\eta| < 0.7$.

In Fig. 4, the measured differential cross section within STAR acceptance, as a function of invariant mass distribution M_X of the central system for $\pi^+\pi^-$, K^+K^- and $p\bar{p}$ is shown. The mass spectrum of the $\pi^+\pi^-$ pairs shows a drop at 1.0 GeV, a clear peak around 1.3 GeV, which is consistent

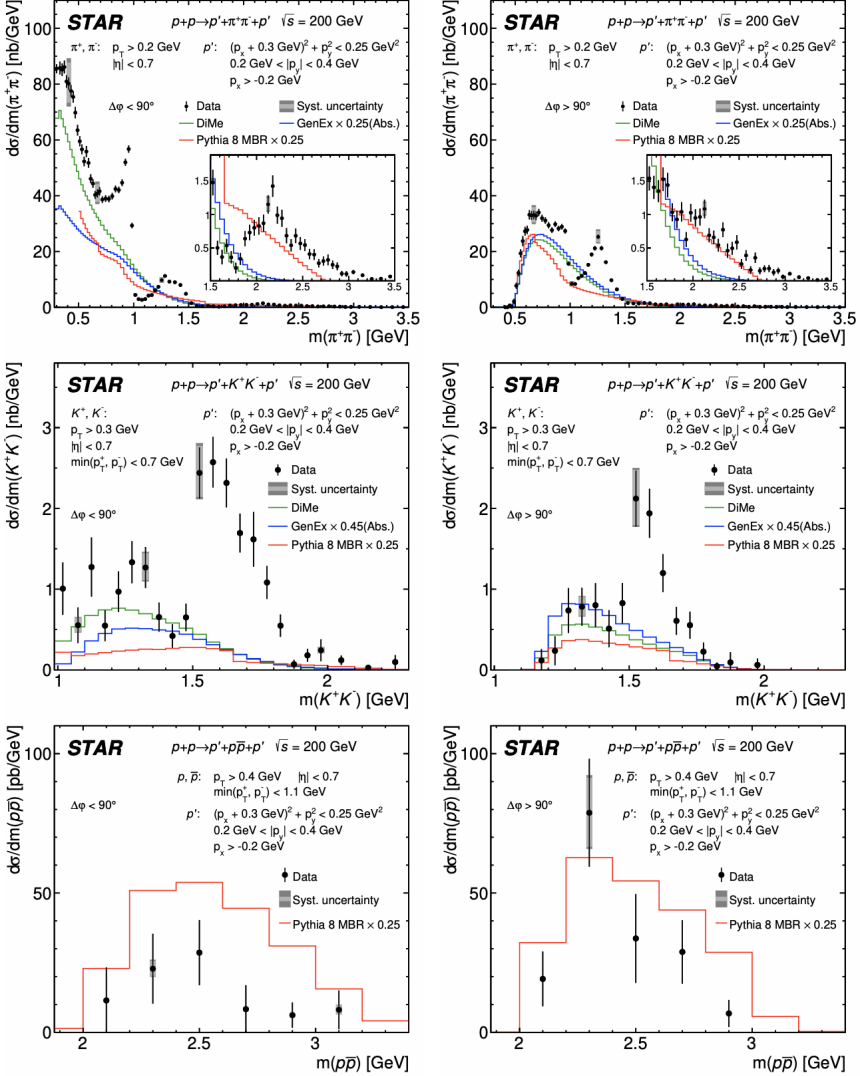


Fig. 4. (Color online) Differential cross sections for CEP of charged particle pairs $\pi^+\pi^-$ (top), K^+K^- (middle) and $p\bar{p}$ (bottom) as a function of the invariant mass of the pair, in two $\Delta\phi$ regions, $\Delta\phi < 90^\circ$ (left column) and $\Delta\phi > 90^\circ$ (right column), measured in the fiducial region explained on the plots. Data are shown as solid points with error bars representing the statistical uncertainties. The typical systematic uncertainties are shown as gray boxes for only a few data points as they are almost fully correlated between neighboring bins. Predictions from three continuum production MC models, GenEx [14], DiMe [15] and PYTHIA 8 MBR [16], are shown as histograms.

with $f_2(1270)$ resonance, and possible further structures at higher masses. The predictions from various Double Pomeron Exchange (DPE) production models of continuum of hadron pairs are also shown.

In Fig. 5, the differential cross section $d\sigma/dm_{\pi^+\pi^-}$ of the invariant mass of $\pi^+\pi^-$ system extrapolated from the fiducial region to the Lorentz-invariant phase space given by the central-state rapidity, $|y_{\pi^+\pi^-}| < 0.4$, and t of the forward protons $0.05 < -t_1, -t_2 < 0.16 \text{ GeV}^2$ is shown. The extrapolated cross section is well described by the continuum production with at least three resonances, the $f_0(980)$, $f_2(1270)$ and $f_0(1500)$, with a possible small contribution from the $f_0(1370)$. The masses and widths of the $f_0(980)$ and $f_0(1500)$ resonances obtained from the fit are in good agreement with the PDG values. The two scalar mesons, $f_0(980)$ and $f_0(1500)$, are predominantly produced at $\Delta\phi < 45^\circ$, whereas the tensor meson $f_2(1270)$ is predominantly produced at $\Delta\phi > 135^\circ$. This allowed fitting the extrapolated differential predominantly produced at $\Delta\phi < 45^\circ$, whereas the tensor meson $f_2(1270)$ is predominantly produced at $\Delta\phi > 135^\circ$.

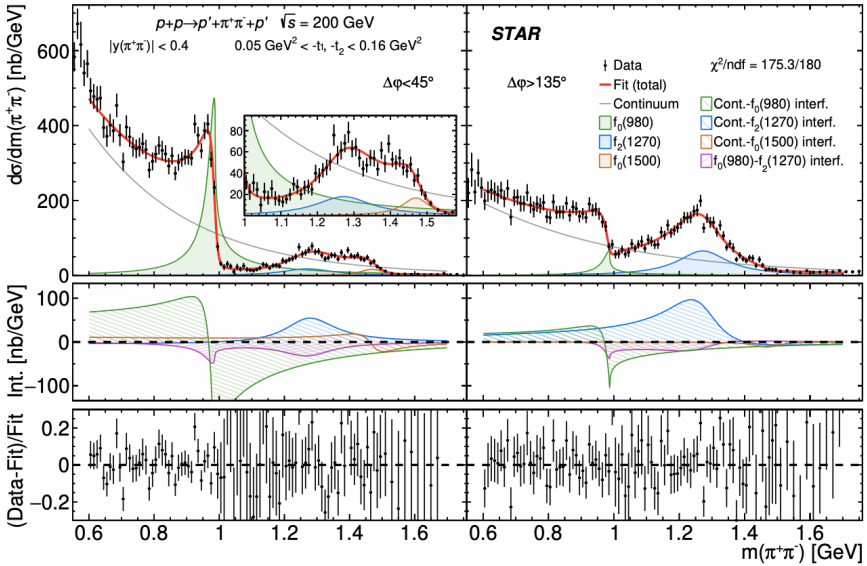


Fig. 5. (Color online) The left and right columns show the cross sections for $\Delta\phi < 45^\circ$ and $\Delta\phi > 135^\circ$, respectively. The data are shown as black points with error bars representing statistical uncertainties. The result of the fit, $F(m)$, is drawn with a solid black/red line. The squared amplitudes for the continuum and resonance production are drawn with lines of different colors, as explained in the legend. The most significant interference terms are plotted in the middle panels, while the relative differences between each data point and the fitted model are shown in the bottom panels.

The phenomenological interpretation of the data requires improvements of the DPE models to consistently include the continuum and resonance-production mechanisms, and the interference between the two, as well as absorption and rescattering effects.

5. Results on particle production at STAR

The next set of results was obtained on particle production in CP and SD processes [17]. The SD process, where one proton stays intact is $pp \rightarrow p + X$, in the CD process $pp \rightarrow p + X + p$ both protons stay intact. In both cases, X denotes a diffractively produced system. An important characteristic is that there is a rapidity gap between the forward protons and the system X . Particle interactions are typically described by QCD-inspired models implemented in Monte Carlo event generators with free parameters that can be constrained by diffractive measurements. Hence, these processes provide insight into the non-perturbative regime of QCD.

Among the results that were obtained were measurements of inclusive charged-particle distributions and identified particle/antiparticle ratios as a function of transverse momentum p_T and η in CD and SD processes. Also, the asymmetry of the production of protons and antiprotons \bar{p}/p ratio at midrapidity in SD and CD were measured.

In Fig. 6, charged particle multiplicities n_{ch} are shown, while in Fig. 7, the p_T distributions are shown. In both cases, a good agreement with the PYTHIA 8 MC generator is shown.

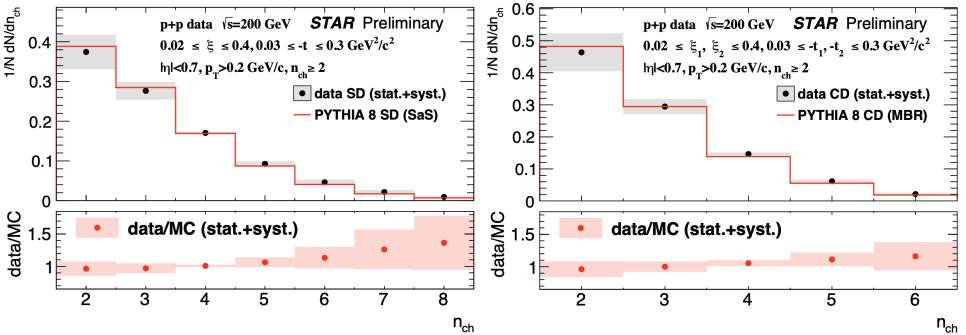


Fig. 6. Multiplicity distributions of primary charged particles for SD (left) and CD (right) processes. Data are compared to PYTHIA 8 simulations.

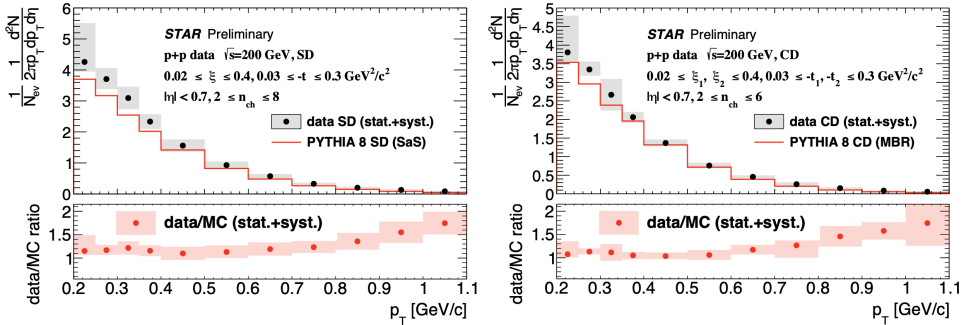


Fig. 7. Charged particles rates as a function of transverse momentum for SD (left) and CD (right) processes. Data are compared to PYTHIA 8 MC simulations.

In Fig. 8, the π^-/π^+ (left) and \bar{p}/p (right) ratios in $|\eta| < 0.5$ interval for CD and SD processes are shown. As expected, the $\pi^-/\pi^+ = 1$, but the $\bar{p}/p < 1$ and that ratio is smaller for SD than CD process. The p_T range is $1 < p_T < 2.2$ GeV/c, where the background from secondaries is small.

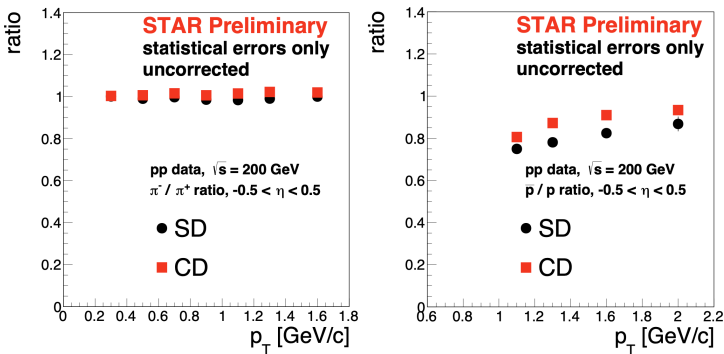


Fig. 8. Comparison of the π^-/π^+ (left) and \bar{p}/p (right) ratios in $|\eta| < 0.5$ interval between CD and SD processes.

6. Future prospects

Two more analyses are ongoing from data on pp scattering at $\sqrt{s} = 510$ GeV: pp elastic scattering and CEP. The preliminary results from the latter were presented at ICHEP 2020 [18]. They are shown in Fig. 9.

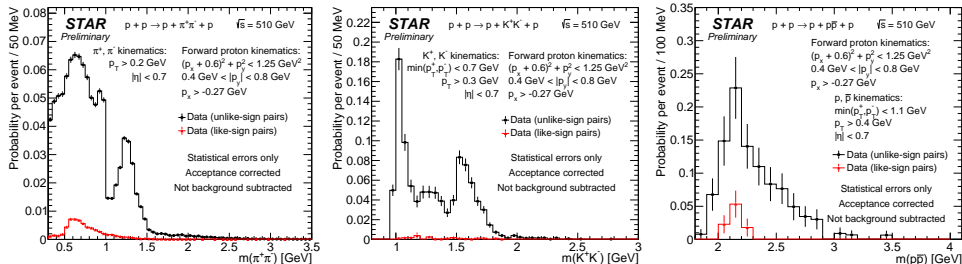


Fig. 9. The invariant mass M_x distributions of $\pi^+\pi^-$ (left), K^+K^- (center) and $\bar{p}p$ (right) for CEP at $\sqrt{s} = 510$ GeV.

7. Summary

We have presented a rich physics program with tagged forward protons at RHIC, which includes topics on number of diffractive processes: elastic scattering, SD, CEP and CP. This specialized program used unique features of the RHIC complex, including polarized proton beams.

REFERENCES

- [1] S. Bültmann *et al.*, «The PP2PP experiment at RHIC: silicon detectors installed in Roman Pots for forward proton detection close to the beam», *Nucl. Instrum. Methods Phys. Res. A* **535**, 415 (2004).
- [2] K.H. Ackermann *et al.*, «STAR detector overview», *Nucl. Instrum. Methods Phys. Res. A* **499**, 624 (2003).
- [3] U. Amaldi *et al.*, «Measurements of the proton–proton total cross section by means of Coulomb scattering at the CERN intersecting storage rings», *Phys. Lett. B* **43**, 231 (1973).
- [4] B.Z. Kopeliovich, A.V. Tarasov, «The Coulomb phase revisited», *Phys. Lett. B* **497**, 44 (2001).
- [5] D. Bernard *et al.*, «The real part of the proton–antiproton elastic scattering amplitude at the centre of mass energy of 546 GeV», *Phys. Lett. B* **198**, 583 (1987).
- [6] S. Bültmann *et al.*, «First measurement of proton–proton elastic scattering at RHIC», *Phys. Lett. B* **579**, 245 (2004).
- [7] S. Bültmann *et al.*, «First measurement of A_N at $\sqrt{s} = 200$ GeV in polarized proton–proton elastic scattering at RHIC», *Phys. Lett. B* **632**, 167 (2006).
- [8] S. Bültmann *et al.*, «Double spin asymmetries A_{NN} and A_{SS} at $\sqrt{s} = 200$ GeV in polarized proton–proton elastic scattering at RHIC», *Phys. Lett. B* **647**, 98 (2007).
- [9] B.Z. Kopeliovich, B.G. Zakharov, «Spin-flip component of the pomeron», *Phys. Lett. B* **226**, 156 (1989).

- [10] N.H. Buttimore *et al.*, «Spin dependence of high energy proton scattering», *Phys. Rev. D* **59**, 114010 (1999).
- [11] L. Adamczyk *et al.*, «Single spin asymmetry A_N in polarized proton–proton elastic scattering at $\sqrt{s} = 200$ GeV», *Phys. Lett. B* **719**, 62 (2013).
- [12] J. Adam *et al.*, «Results on total and elastic cross sections in proton–proton collisions at $\sqrt{s} = 200$ GeV», *Phys. Lett. B* **808**, 135663 (2020).
- [13] J. Adam *et al.*, «Measurement of the central exclusive production of charged particle pairs in proton–proton collisions at $\sqrt{s} = 200$ GeV with the STAR detector at RHIC», *J. High Energy Phys.* **2007**, 178 (2020).
- [14] R.A. Kycia *et al.*, «GenEx: A Simple Generator Structure for Exclusive Processes in High Energy Collisions», *Commun. Comput. Phys.* **24**, (2018).
- [15] L.A. Harland-Lang *et al.*, «The phenomenology of central exclusive production at hadron colliders», *Eur. Phys. J. C* **72**, 2110 (2012).
- [16] R. Ciesielski, K. Goulianos, «MBR Monte Carlo Simulation in PYTHIA 8», [arXiv:1205.1446](https://arxiv.org/abs/1205.1446) [hep-p].
- [17] L. Fulek, «Measurements of Particle Spectra in Diffractive Proton–Proton Collisions with the STAR Detector at RHIC», *Acta Phys. Pol. B Proc. Suppl.* **12**, 999 (2019).
- [18] STAR Collaboration (T. Truhlar), «Study of the central exclusive production of $\pi^+\pi^-$, K^+K^- and $p\bar{p}$ pairs in proton–proton collisions at $\sqrt{s} = 510$ GeV with the STAR detector at RHIC», [arXiv:2012.06295](https://arxiv.org/abs/2012.06295) [hep-ex].